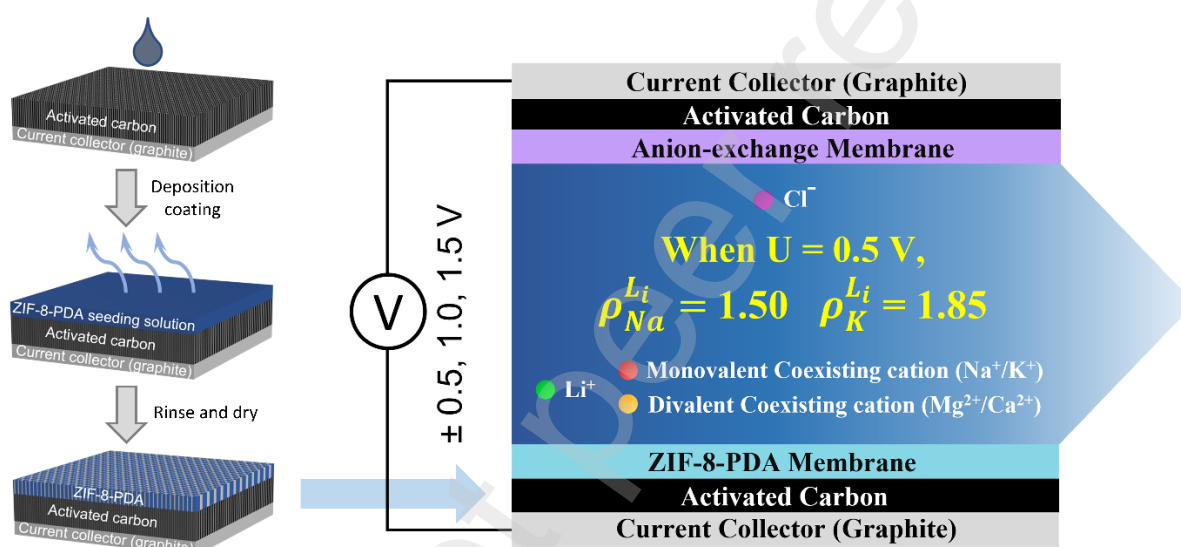


29 of applied potentials on Li extraction performances. The results indicated advantages for Li
 30 extraction when coexisting cations were monovalent than divalent. Additionally, a lower
 31 voltage of 0.5 V could provide superior Li selectivity, charge efficiency (CE), and energy
 32 normalized to Li (ENL) than higher voltages. Especially, Li selectivity of 1.50 and 1.85 was
 33 achieved in Li/Na and Li/K feeds under 0.5 V, 37% and 74% higher than those under 1.5 V,
 34 respectively, illuminating the potential of MCDI for Li extraction from SWRO brine with low
 35 energy input.

36

37 Graphical abstract



38

39

40 **Keywords:** Lithium extraction; Zeolitic imidazolate framework-8; Membrane capacitive
 41 deionization; Ion-selective membrane; Mono and divalent cations

42 **1. Introduction**

43 Lithium (Li), one of the key elements applied in electric vehicles and mobile devices, has
44 become highly demanded, prompted by the rapid development of the lithium-ion battery
45 industry [1, 2]. From 2010 to 2021, global Li consumption boomed nearly 4 times, from 24.5
46 kt to 93.0 kt [3, 4]. Given that over 99.9% of Li is reserved in the ocean and about 75% of Li
47 on land is stored in brine, it is of great value to recover Li from aqueous resources from a
48 business perspective and develop eco-friendly Li extraction materials and processes from an
49 environmental perspective.

50 Conventional approaches to selectively extracting Li from brine include solvent extraction and
51 adsorption [5, 6]. Whereas solvent extraction can separate Li from brine with a high Mg/Li
52 ratio, the lifespan of the equipment can be limited due to the corruption of organic solvents,
53 and the disposal of solvent leakage can be complicated. Adsorption is widely studied and has
54 been applied in the real-world industry due to the merits of low cost, high Li selectivity, and
55 simple operation process [7], but the processes of adsorbent granulation and ad/desorption are
56 time-consuming. In addition, the acid stripping process for adsorbent regeneration can produce
57 hazardous secondary waste.

58 To further overcome the drawbacks of conventional approaches and improve Li extraction
59 efficiency, Li separation performances, and environmental friendliness, emerging technologies,
60 for example, electrochemical [8-11] and membrane-based processes [12, 13] have been paid
61 more considerable attention in the past decade. Electrodialysis (ED) can separate monovalent
62 and multivalent ions efficiently combined with nanofiltration (NF) membranes [13, 14] and
63 ion-exchange membranes (IEM) [15, 16]. However, the high energy inputs weaken its
64 economic feasibility. What is more, the separation of Li and other monovalent metal ions is
65 still challenging. In contrast, capacitive deionization (CDI), a novel environmental-friendly
66 technology for facile desalination depending on the electrosorption process [17-19], presents
67 great benefits of technical simplicity, affordable cost, mild operation conditions, and low
68 energy inputs. It takes advantage of low voltages (usually ≤ 1.5 V), impelling cations and
69 anions towards the oppositely charged electrodes composed of two porous electrode materials
70 characterized by a high specific surface area. Then the temporarily adsorbed ions are released
71 into the solution by a reverse charge [17]. This technology has attracted increasing attention in
72 this century and is regarded as a promising solution to ion removal, energy harvesting, water
73 purification, and resource recovery as a next-generation technology [20-22].

74 The research on Li recovery using CDI systems focused on material synthesis, electrode
75 fabrication, cell architecture design, and operation process enhancement. Ion selectivity can be
76 determined by the effect of ion size and valence on the diffusion rate under an electric field
77 [23, 24], and the pore-size distribution of electrode materials can affect salt adsorption capacity
78 and ion selectivity [25, 26]. Nevertheless, the electrode materials are reported as a critical factor
79 influencing CDI performances [24, 27, 28]. Manganese oxide-based electrodes are widely
80 studied because of their extraordinary Li selectivity [27, 29, 30]. Other metal oxide-based
81 electrodes, e.g., Li_3VO_4 and Co_3O_4 , also exhibited outstanding adsorption performance [31,
82 32]. Some research emphasized CDI process enhancement by evaluating various working
83 modes and optimizing operation conditions of feed concentrations and flow rates [33, 34]. In
84 addition, the investigation of novel CDI cell architectures highlights membrane CDI (MCDI),
85 flow-electrode CDI (FCDI), and hybrid CDI (HCDI) [35-38]. Particularly, MCDI, a
86 modification of classical CDI by introducing ion-exchange membranes (IEM) or ion-selective
87 membranes (ISM) between two opposite electrodes, can avoid co-ion repulsion, reduce anode
88 oxidation and energy consumption, increase deionization efficiency and adsorption capacity,
89 and work with low-concentration solutions (≤ 20 mM) [39, 40]. The incorporation of
90 membranes can tune the pore size distribution of an electrode or adjust chemical contacts with
91 target ions, improving ion selectivity.

92 Currently, metal-organic frameworks (MOFs) have gained great interest in the fabrication of
93 ion-selective membranes. They are organic-inorganic hybrid materials with intermolecular
94 pores formed by self-assembling organic ligands and inorganic metal ions or clusters through
95 coordination bonds [41]. After originally proposed by Yaghi in 1995, MOFs were reported
96 with many subclasses, such as UiOs, Materials of Institute Lavoisier frameworks (MILs), and
97 zeolitic imidazolate frameworks (ZIFs) [42]. ZIF families, built by metal ions, such as zinc
98 (Zn) and cobalt (Co) ions, and nitrogen atom-linked ditopic imidazole anions, have been widely
99 utilized in gas storage and separation, resource recovery, catalysis, sensing, and drug
100 transportation due to their abundant designable structural types, low density, permanent holes,
101 high specific surface area, and functional hole space [43-46]. Especially, ZIF-8 is
102 acknowledged as a promising material for metal recovery applications as it has a homogeneous
103 porosity appearance with substantial surface areas [47]. Zhang et al. confirmed the possibility
104 of three-dimensional ZIF-8 membranes for Li separation. The simulation study revealed that
105 the ionic dehydration-rehydration interactions in sub-nano pore channels could contribute to
106 the difference in ion-transport rates [48]. Based on this mechanism, Mohammad et al.

107 fabricated a ZIF-8-based composite membrane for Li extraction, which could separate
108 monovalent and divalent ions [49]. However, separating Li from other monovalent cations is
109 still challenging. Hossain et al. prepared AC/ZIF-8 and AC/ZIF-8/CEM cathodes for CDI
110 systems by coating ZIF-8 double layers on activated carbon (AC) electrodes via an in-situ
111 growth method. Their electrosorption results demonstrated successful separations of Li from
112 Na/K coexisting binary solutions [50].

113 Nevertheless, ZIF-8 was reported to easily hydrolyze into zinc and imidazolate ions within 24
114 h in aqueous solutions due to the weak bonds of metal nodes and ligands [51]. The poor hydro-
115 stability would limit its long-time applications in water treatment. Thus, many strategies were
116 proposed for ZIF-8 modification to address the water stability problem, such as surface ligand
117 exchange with 5,6-dimethylbenzimidazole (DMBIM) [52, 53] and surface functionalization by
118 incorporating deoxyribonucleic acid (DNA)/polydopamine (PDA) [54, 55]. PDA, a mussel-
119 inspired adhesive cross-linker that can be easily obtained through dopamine (DA) self-
120 polymerization at alkaline aerobic conditions, can tether N and O containing materials by
121 forming covalent and noncovalent bonds [56, 57]. By encapsulating ZIF-8 nanoparticles in
122 PDA, hydrolysis could be inhibited since water molecules would form hydrogen bonds with
123 hydroxyl groups on the surface and difficultly enter the interior of ZIF-8 [58].

124 Based on the considerations above, we employed PDA as an adhesive to bind ZIF-8 crystals
125 strongly. The composite ZIF-8-PDA membrane was doubly coated on commercial AC
126 electrodes via a deposition coating method. The fabricated AC/ZIF-8-PDA electrodes were
127 assembled into a batch MCDI setup as cathodes while anion exchange membrane (AEM)-
128 coated electrodes were used as the counter ones. This study investigated the Li extraction
129 performances of the MCDI system using diluted binary brines (containing Li and M; M
130 representing Na, K, Mg, and Ca) as feeds. In addition, the MCDI tests were conducted with
131 voltages of ± 0.5 V, ± 1.0 V, and ± 1.5 V to study the influence of applied voltages on Li
132 selectivity, Li adsorption capacity (LAC), charge efficiency (CE), and energy normalized to Li
133 (ENL). Overall, this work broadened the use of ZIF-8 for AC electrode modification and
134 validated the MCDI technology as a promising method for Li recovery from diluted brine.

135 **2. Materials and methods**

136 **2.1 Materials**

137 The materials for ZIF-8-PDA synthesis included zinc nitrate hexahydrate ($\text{N}_2\text{O}_6\text{Zn}_6\cdot\text{H}_2\text{O}$,
138 molar mass: 297.49 g/mol), solvent 2-Methylimidazole (2-mIM) ($\text{C}_4\text{H}_6\text{N}_2$, molar mass: 82.10
139 g/mol), methanol (CH_3OH , molar mass: 32.04 g/mol, suitable for HPLC),
140 Tris(hydroxymethyl)aminomethane (Tris) ($\text{NH}_2\text{C}(\text{CH}_2\text{OH})_3$, molar mass: 121.14 g/mol), and
141 dopamine hydrochloride ($(\text{HO})_2\text{C}_6\text{H}_3\text{CH}_2\text{CH}_2\text{NH}_2\cdot\text{HCl}$, molar mass: 189.64 g/mol) were
142 provided by Sigma Aldrich.

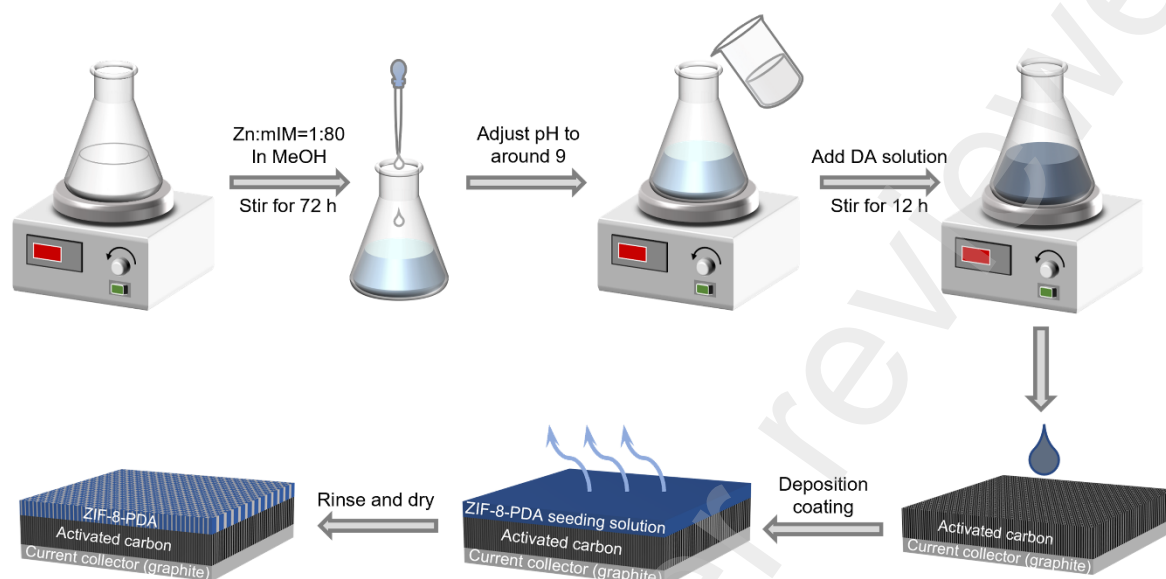
143 The binary feed solutions were prepared using lithium chloride (LiCl, molar mass: 42.39 g/mol,
144 reagent grade), sodium chloride (NaCl, molar mass: 58.44 g/mol), potassium chloride (KCl,
145 molar mass: 74.55 g/mol), anhydrous magnesium chloride (MgCl_2 , molar mass: 95.21 g/mol),
146 and anhydrous calcium chloride (CaCl_2 , molar mass: 110.98 g/mol) obtained from Sigma
147 Aldrich.

148 For the assembly of the MCDI setup, the acryl unit cell, AC electrodes, and AEM-coated AC
149 electrodes were collected from Siontech Co., Ltd. Whatman glass fiber prefilters with 2- μm
150 pores were employed in MCDI cells as the spacers. Milli-Q (MQ) water was utilized to produce
151 feed solutions. All compounds in the experiments were utilized as supplied without additional
152 purification.

153 **2.2 Preparation of AC/ZIF-8-PDA electrodes**

154 The schematic illustration of the electrode preparation process is depicted in **Fig. 1**. ZIF-8
155 crystals were synthesized in methanol at room temperature for 72 h, according to a number of
156 published papers [59, 60]. The precursor solution for ZIF-8 growth was prepared by mixing
157 1.2 g of $\text{Zn}(\text{NO}_3)_2\cdot 6\text{H}_2\text{O}$ and 26.62 g of 2-Methylimidazole in 150 mL of methanol in a beaker
158 under magnetic stirring for 72 h. The pH of the ZIF-8 seeding solution was adjusted to alkaline
159 (around 9) with Tris. For ZIF-8-PDA synthesis, 0.6 g of dopamine hydrochloride was dissolved
160 in 50 mL methanol, then mixed with ZIF-8 seeding solution followed by stirring for 12 h.
161 Before electrode modification, ZIF-8-PDA was washed three times using methanol to remove
162 superfluous 2-mIM and PDA and was stored in methanol. Then, the deposition coating method
163 was adopted twice under room temperature for electrode coating, transferring 30 mL of the
164 ZIF-8-PDA seeding solution mentioned above per time on the AC electrode fixed by a square

165 acrylic mold of 100 cm² internal diameter and waiting until the solvent was fully evaporated.
166 Subsequently, the electrode was rinsed thrice with methanol and MQ water, respectively, and
167 dried at room temperature. The fabricated electrodes were preserved in a desiccator before use.



168
169 **Figure 1.** Schematic illustration of ZIF-8-PDA synthesis and AC/ZIF-8-PDA electrode
170 fabrication.

171 2.3 Characterization

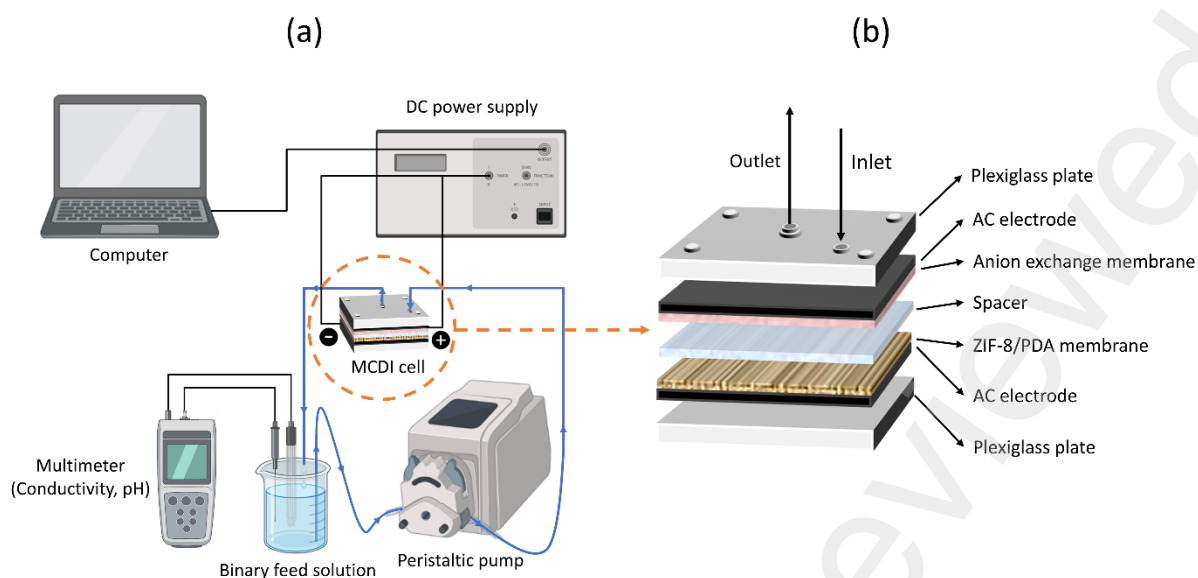
172 The morphologies of ZIF-8-PDA particles, bare AC electrode surface, and the membrane
173 surface along with the cross-section of AC/ZIF-8-PDA electrode were characterized by
174 scanning electron microscopy (SEM, Zeiss Supra 55VP). The elemental compositions of the
175 ZIF-8-PDA layer were measured using an energy-dispersive X-ray spectroscopy detector (EDS,
176 Oxford). The chemical composition and functional groups of the ZIF-8 and ZIF-8-PDA
177 particles were recognized using Fourier transform infrared (FT-IR) spectroscopy (IRPrestige-
178 21) in the wavenumber range of 400 – 4000 cm⁻¹. The crystalline phases of ZIF-8 particles
179 were identified by X-ray powder diffractometer (XRD, Bruker D8 Discover) with Cu K α
180 radiation source at a scanning rate of 0.04°/s from 0.5° to 50°. The nitrogen isotherm
181 measurement was performed with a Quantachrome Analyzer (Micromeritics TriStar II Plus,
182 Australia). The ZIF-8-PDA particle sample was degassed for 10 h at 150 °C. The Brunauer–
183 Emmett–Teller (BET) method was used to determine the specific surface area of ZIF-8-PDA
184 particles. The pore size distribution was analyzed based on the non-local density functional
185 theory (DFT), and the total volume was measured at a relative pressure (P/P₀) over 0.99.

186 2.4 Static water stability verification of ZIF-8-PDA

187 The water stability test was conducted by immersing ZIF-8-PDA particles in water and
188 observing the transformations of morphology and crystalline phase, following the published
189 studies towards MOF water stability [61, 62]. It was reported that the hydrolysis of ZIF-8 can
190 be reflected in the morphology shift from diamond dodecahedron to leaf shape [63]. The ZIF-
191 8-PDA particles were added into Milli-Q water at predetermined ratios of 2 wt%, 5 wt%, 10
192 wt%, and 20 wt% and soaked for 24h. Later, the particles were collected by centrifuging at a
193 rate of 4000 rpm/min for 10 mins, removing water, and drying in an oven at 60°C overnight.
194 The morphologies of the obtained water-soaked particles were monitored by SEM. In addition,
195 XRD patterns of the ZIF-8-PDA particles fully soaked in water for one month and the ZIF-8
196 soaked for one day were measured and compared with pristine ZIF-8-PDA peaks.

197 2.5 MCDI setup

198 A diagram of the lab-scale MCDI module and cell is presented in **Fig. 2**. The MCDI system
199 (**Fig. 2a**) consisted of a potentiostat for providing constant charge potentials, a computer for
200 recording and analyzing the data of current, voltage, power, and resistance, a multimeter for
201 monitoring pH and conductivity, an MCDI cell for electrosorption, a reservoir containing
202 binary feed solution, and a peristaltic pump for circulating the solution flow in the system. The
203 multimeter measured and recorded the real-time data every 10 seconds. The peristaltic pump
204 was set to a constant flow rate (20 mL/min). 1 mL of effluent samples were collected from the
205 solution reservoir every 2 or 5 mins for cation composition analysis. The potentiostat (Autolab
206 PGSTAT302N, Metrohm) delivered charging potentials of -0.5 V, -1.0 V, and -1.5 V in the
207 electro-adsorption process for Li extraction and discharge potentials of 0.5 V, 1.0 V, and 1.5 V
208 in the electro-desorption processes for ion recovery and electrode regeneration. The binary feed
209 solutions contain 10 mM LiCl and MCl_x (M = associated coexisting cations (Na, K, Mg, or
210 Ca), $x = 1$ or 2). As **Fig. 2b** shows, the assembly of the MCDI cell comprised an AC/ZIF-8-
211 PDA electrode, an AC/AEM (thickness of 170 μm) electrode, and a glass fiber spacer
212 (Whatman, thickness of 250 μm). The solution flowed in the assembly from the edge, then
213 down the spacer channel, and finally out via the central outlet. 20-min cycles were repeated
214 trice for the electrosorption/desorption tests with each type of feed solution.

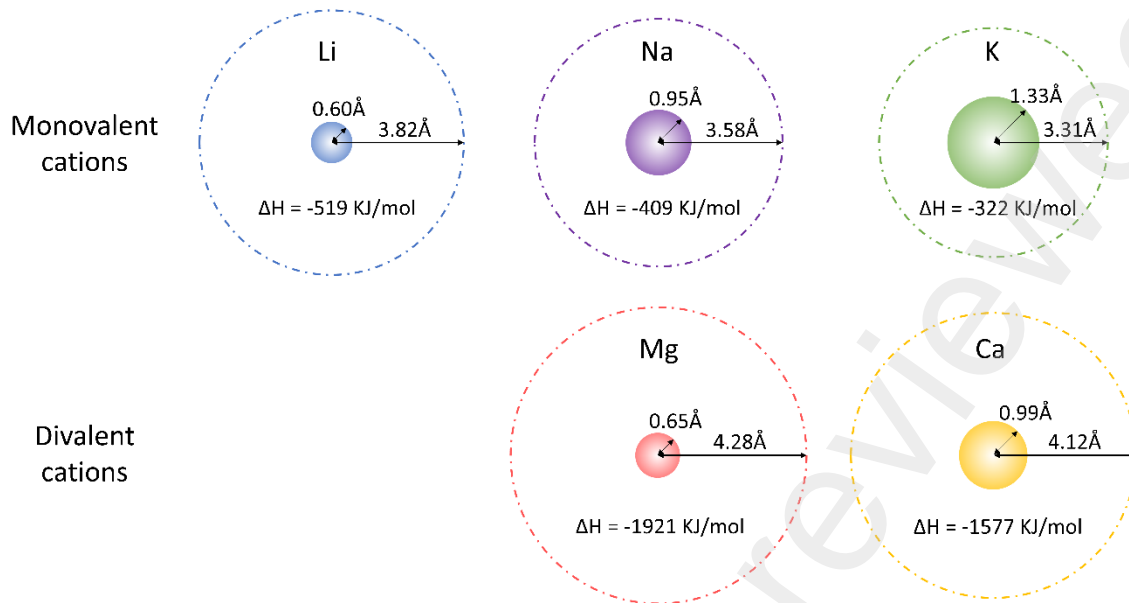


215

216 **Figure 2.** Schematic illustration of the experimental design.

217 **2.6 Li extraction test under different voltages**

218 Li extraction performances were tested using the MCDI system with constant hydraulic
 219 residence times and a series of equimolar binary feed solutions containing Li and M (M
 220 representing the associated coexisting cations). To compare the competing ion removal in the
 221 electrosorption process, four mono and divalent alkali and alkali earth metals with similar ionic
 222 sizes to Li were selected as coexisting cations, i.e., Na, K, Mg, and Ca. Na and K are abundant
 223 in seawater reverse osmosis (SWRO) brine, and Mg and Ca are core competitors in Salt Lake
 224 brine. The MCDI tests using Li/Na and Li/K binary feed are named monovalent cases, and
 225 those using Li/Mg and Li/Ca binary feed are appointed divalent cases. The bare and hydrated
 226 ionic radii and their hydration enthalpy are listed in **Fig. 3**. An initial concentration of 10 mM
 227 for each component and a volume of 200 mL were fixed for all feed solutions.



228
 229 **Figure 3.** The bare and hydrated ionic radius of Li, Na, K, Mg, and Ca and their hydration
 230 enthalpy [64, 65].

231 The electrosorption processes were firstly carried out at a voltage of -1.0 V, and the subsequent
 232 desorptions were at 1.0 V. The duration of adsorption and desorption was both set to 20 min.
 233 The effluent samples of 1 mL were collected every 2 mins during the electrosorption phase. To
 234 investigate the influence of applied voltages on Li adsorption performance, the MCDI
 235 experiments were conducted under $\pm 0.5V$ and $\pm 1.5V$. The concentrations of cations in the
 236 samples were measured by inductively coupled plasma mass spectrometry (ICP-MS, Agilent
 237 7900, Agilent Technologies Inc.). The real-time conductivity and pH of the solutions were
 238 monitored every 10 seconds. The tests were repeated three times, and the standard average was
 239 calculated. Li extraction performances were evaluated in terms of ion removal rate, Li
 240 selectivity, LAC, CE, and ENL.

241 The ion removal rate was calculated with Eq. (1).

$$242 \quad \eta_x(\%) = \left(1 - \frac{C_t}{C_0}\right) \times 100 \quad (1)$$

243 Where x is Li, Na, K, Mg, or Ca; η_x is the ion removal rate of x; C_0 is the initial concentration
 244 of x; C_t is the concentration of x at time t.

245 The Li selectivity was calculated with Eq. (2).

$$246 \quad \rho_M^{Li} = \frac{\eta_{Li}}{\eta_M} \quad (2)$$

247 Where M represents the competing cation (Na, K, Mg, or Ca) and ρ_M^{Li} is the relative Li
248 selectivity to M.

249 Li adsorption weight (LAW) is described as Li removal weight per 100 cm² of the cathode,
250 given by Eq. (3), and LAC is defined as the final LAW at the end of each adsorption experiment,
251 i.e., the weight of adsorbed Li per 100 cm² of the cathode.

$$252 \text{ LAW}_t \text{ (mg)} = (C_0 - C_t)V \quad (3)$$

253 Where V is the feed solution volume.

254 The CE (Λ) and ENL were calculated by Eq. (4) and (5), respectively.

$$255 \Lambda \text{ (\%)} = \frac{(C_t - C_0)VF}{M_{Li}Q} \times 100 \quad (4)$$

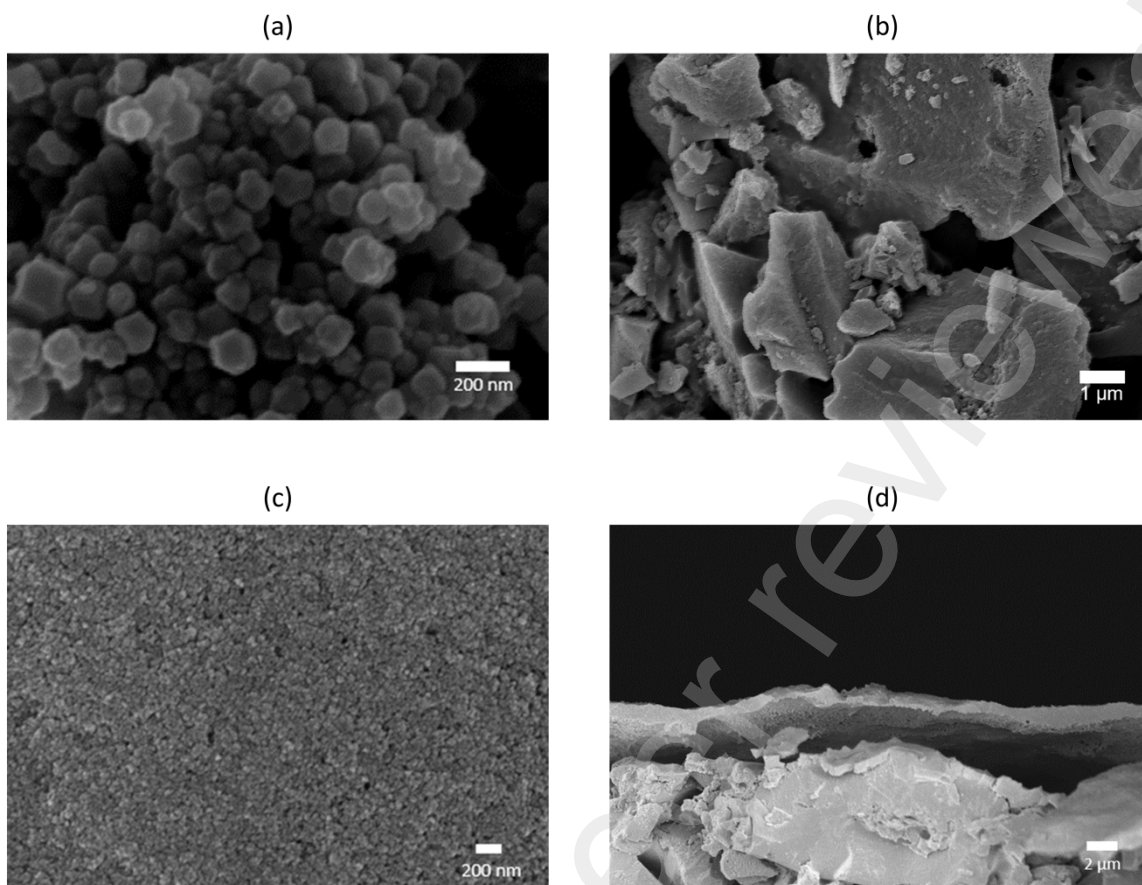
$$256 \text{ ENL } (\mu\text{mol J}^{-1}) = \frac{(C_t - C_0)V}{M_{Li}E_{ad}} = \frac{(C_t - C_0)\int I dt}{M_{Li}} \quad (5)$$

257 Where F is the Faraday constant (96485 C mol⁻¹); M_{Li} is the molar mass of Li (6.94 g mol⁻¹);
258 Q is the charge supplied per adsorption cycle (C); E_{ad} is the energy supplied during an
259 adsorption cycle during constant voltage MCDI.

260 **3. Results and discussion**

261 **3.1 Characterizations of ZIF-8-PDA particles and the modified electrode**

262 **Fig. 4** shows SEM images of ZIF-8 particles, the bare AC electrode, and the surface and cross-
263 section of the AC/ZIF-8-PDA electrode. Ultrasmall ZIF-8-PDA particles with the shape of
264 diamond dodecahedrons were synthesized. The bare AC electrode showed an uneven and
265 porous surface composed of AC lumps with varied sizes, which corresponds with published
266 work [66]. The thickness of the carbon layer on the graphite foil was estimated to be 100 μm .
267 After deposition coating, a dense ZIF-8-PDA layer of around 1 μm thick on average fully
268 covered the top of the AC electrode.

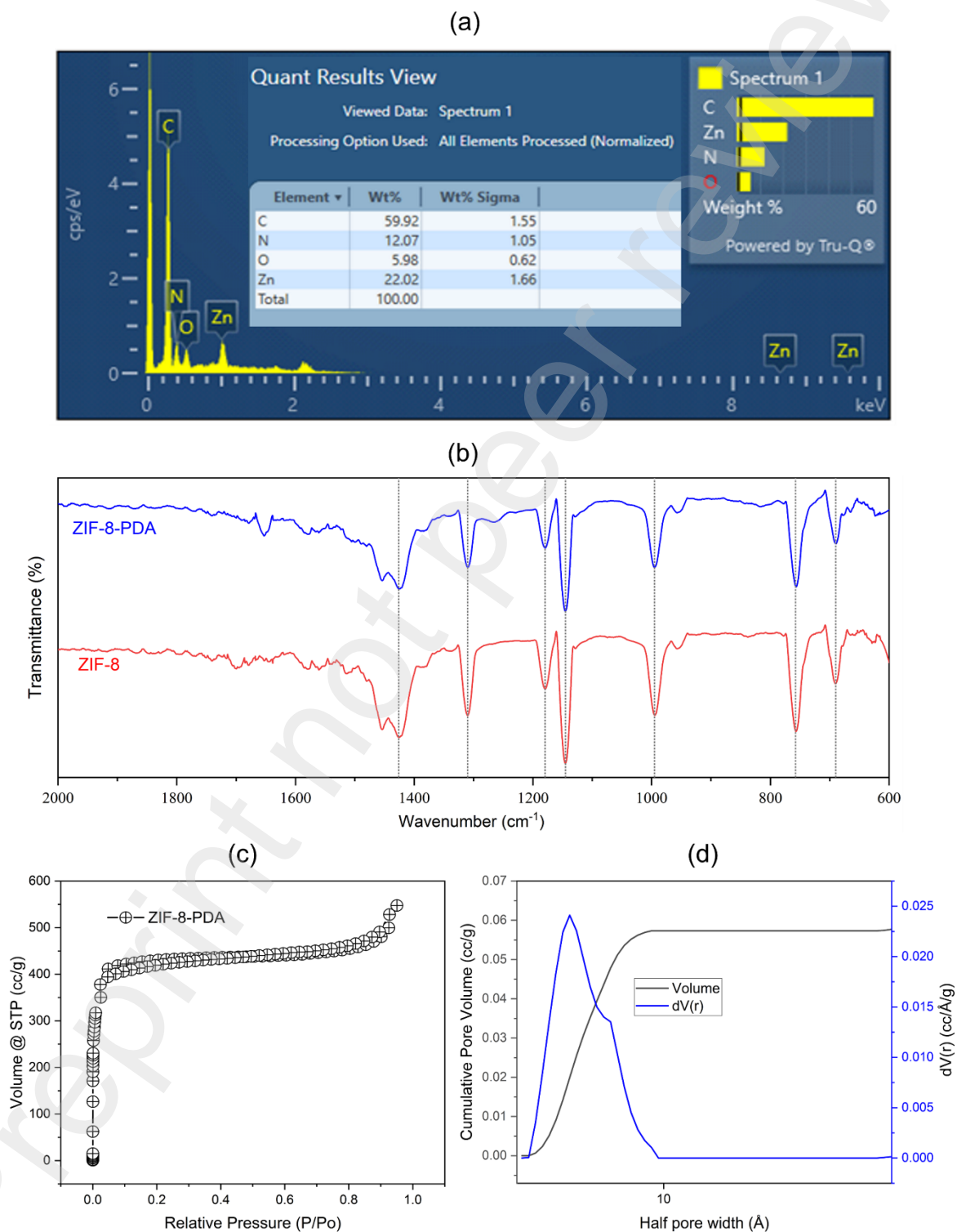


269

270 **Figure 4.** SEM images of (a) ZIF-8-PDA particles, (b) bare AC electrode, (c) the surface of
 271 the AC/ZIF-8-PDA electrode, and (d) the cross-section of the AC/ZIF-8-PDA electrode.

272 The information on the functional groups, element components, micropores, and crystalline
 273 phases of ZIF-8-PDA were illustrated in **Fig. 5** and **Fig. 7(c)**, given by FTIR, EDS, BET, and
 274 XRD characterizations. The EDS results confirmed the composition of carbon (59.92%),
 275 nitrogen (12.07%), oxygen (5.98%), and zinc (22.02%) in ZIF-8-PDA. In the FTIR spectra of
 276 ZIF-8 and ZIF-8-PDA, the peaks at 690 and 758 cm^{-1} were associated with Zn-N and Zn-O
 277 bonds, respectively; peaks between 990 and 1500 cm^{-1} could be accredited to in-plane and out-
 278 of-plane C-N stretching vibration in imidazole groups, and the peaks at 1580 cm^{-1} were related
 279 to C=N bonds [67-69]. The type-I nitrogen adsorption isotherm for ZIF-8-PDA showed a
 280 dynamic increase in adsorbed N_2 at low relative pressure, indicating the presence of intrinsic
 281 micropores. The effective BET surface area of ZIF-8-PDA was estimated to be 175.87 m^2/g ,
 282 and the pore volume was evaluated as 0.12 cm^3/g . The half pore width of ZIF-8-PDA was
 283 calculated to be within 10Å, which could be the main contributor to ion separation. The
 284 incorporation of PDA altered the pore size distribution. Compared to ZIF-8, of which the
 285 surface area could be larger than 1000 m^2/g [46], ZIF-8-PDA showed low porosity yet wider

286 pore widths, which could weaken Li sieving performance. The XRD peaks of ZIF-8-PDA
 287 particles were identified at the 2-theta positions of 7.39° (110), 10.40° (200), 12.75° (211),
 288 14.75° (220), 16.50° (310), 18.06° (222), corresponding to characteristic peaks of ZIF-8 in
 289 literature [53, 55, 58, 60], implying that the crystal structure of ZIF-8 remained intact with the
 290 incorporation of PDA.

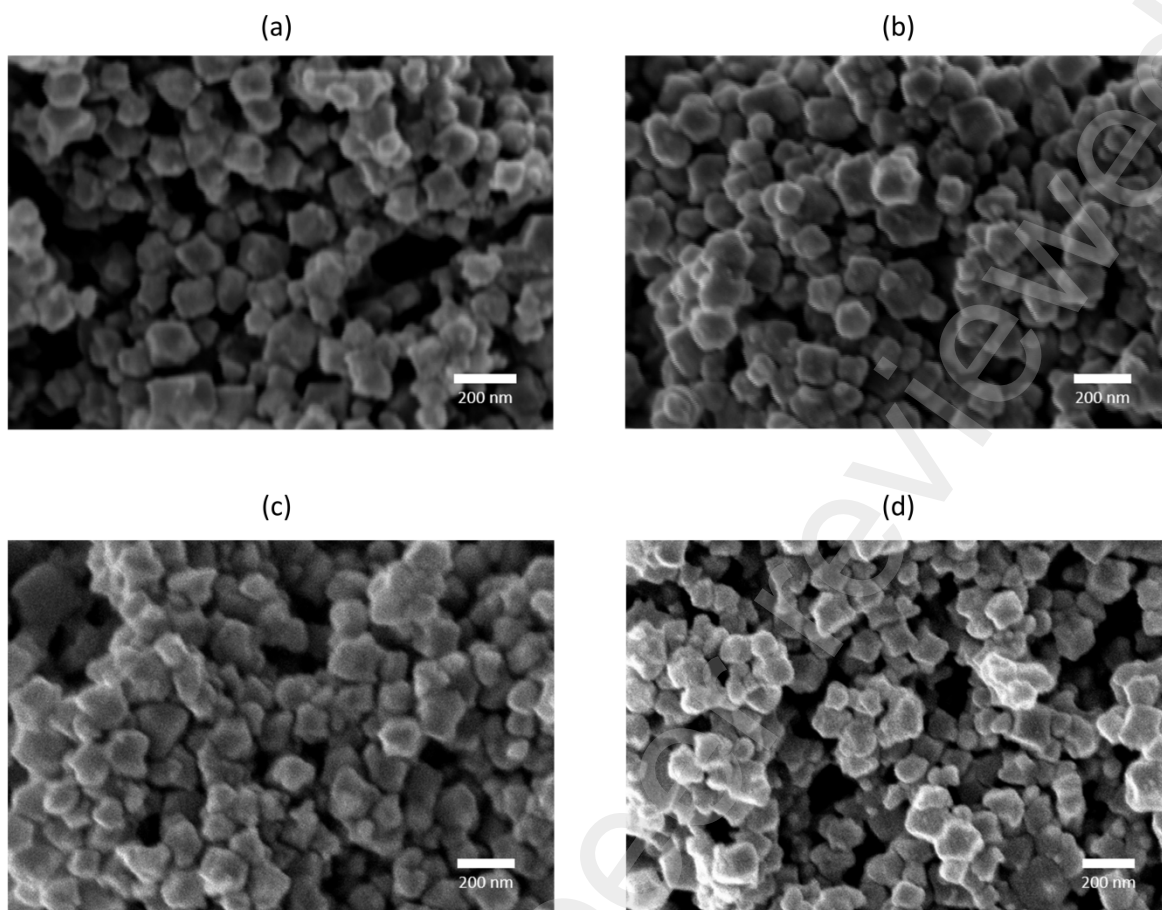


291
 292 **Figure 5.** (a) EDS, (b) FTIR patterns, (c) BET analysis, and (d) pore size of the ZIF-8-PDA.

293 3.2 Water stability of the ZIF-8-PDA particles

294 **Fig. 6** shows the morphologies of the ZIF-8-PDA particles after being immersed in water for
295 24 h. It can be observed that although some particles changed to smaller spherical and irregular
296 forms, most of the particles kept the original morphology. The degradation proportion slightly
297 increased with the decrease in MOF/water ratio. **Fig. 7** demonstrates SEM images and XRD
298 patterns of the ZIF-8 and ZIF-8-PDA particles after soaking in MQ water for 24 h and one
299 month, respectively. The hydrolyzed ZIF-8 presented leaf- and needle-like shapes,
300 corresponding to other research on ZIF-8 hydrostability [53, 63]. In comparison, the
301 morphology transformation degree of ZIF-8-PDA was much slighter. For XRD results (**Fig.7c**),
302 the crystallinity of the (110) phase reduced significantly, those of the (310) and (222) phases
303 increased, and some unknown peaks appeared with the hydrolysis. Notably, the (100) phase of
304 ZIF-8 almost disappeared, and the positions of many peaks shifted. SEM and XRD results
305 suggested a better water stability of ZIF-8-PDA than ZIF-8, which can be attributed to the
306 protection of PDA. The hydrolysis occurs when ZIF-8 contacts with water molecules, but the
307 presence of PDA could provide a relatively restrained environment to the inner ZIF-8 particles,
308 inhibiting escaping of the hydrolyzed Zn^{2+} and 2-mIM and favoring the re-formation of ZIF-8.
309 The concentrations of Zn^{2+} and 2-mIM could be much higher in the PDA-restrained zone than
310 in water, in which a dynamic equilibrium between ZIF-8 formation and hydrolysis might exist.

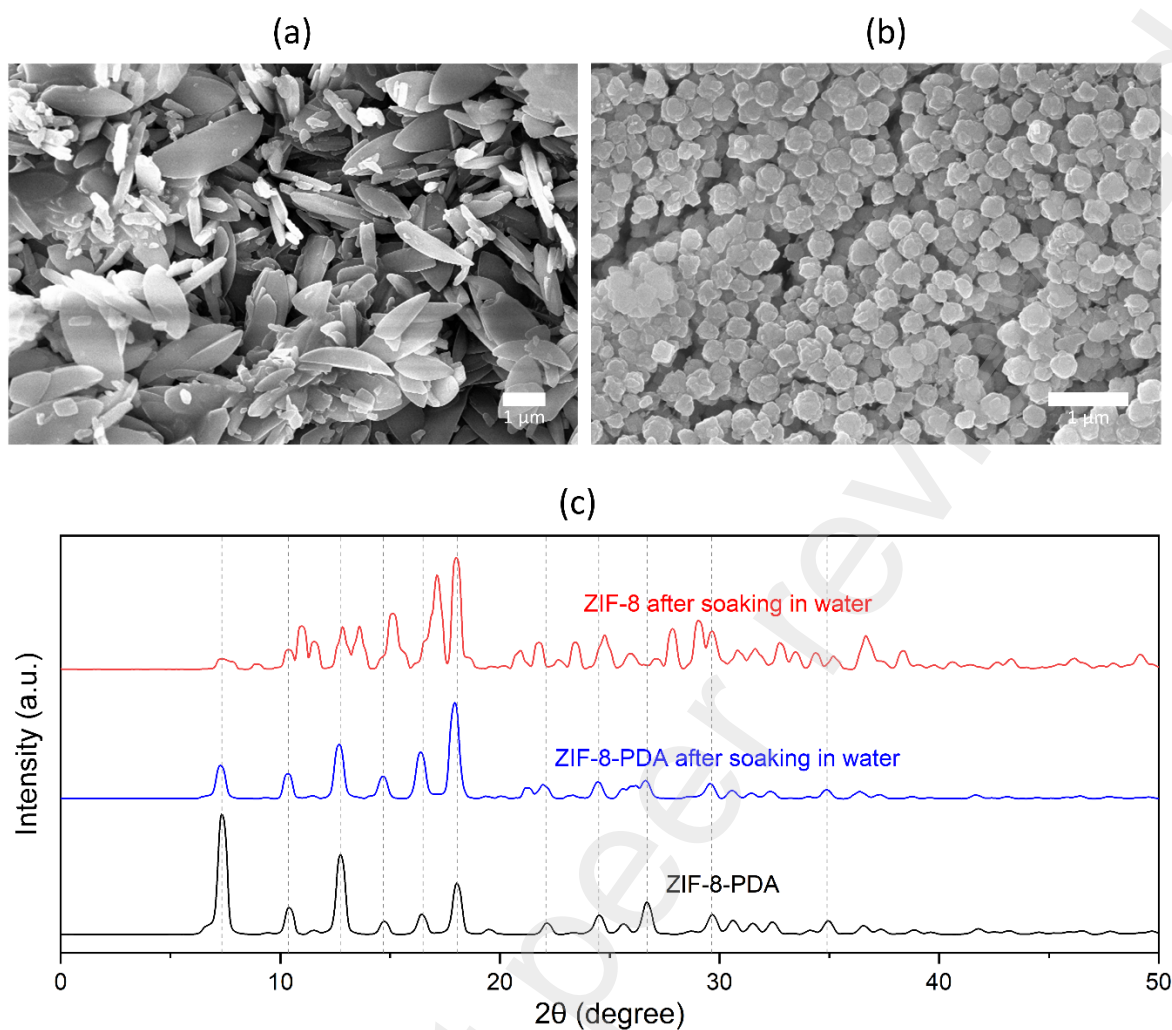
311



312

313 **Figure 6.** SEM images of ZIF-8-PDA particles mixed with MQ water after 24 h by MOF/water
314 weight ratios of (a) 1:5, (b) 1:10, (c) 1:20, (d) 1:50.

315



316

317 **Figure 7.** SEM images of (a) hydrolyzed ZIF-8 particles after soaking in MQ water for 24 h
 318 and (b) ZIF-8-PDA particles after soaking in MQ water for one month, and (c) XRD patterns
 319 of the above ZIF-8 and ZIF-8-PDA after soaking in water.

320 3.3 MCDI performance under different voltage conditions

321 3.3.1 MCDI performance under 1.0 V

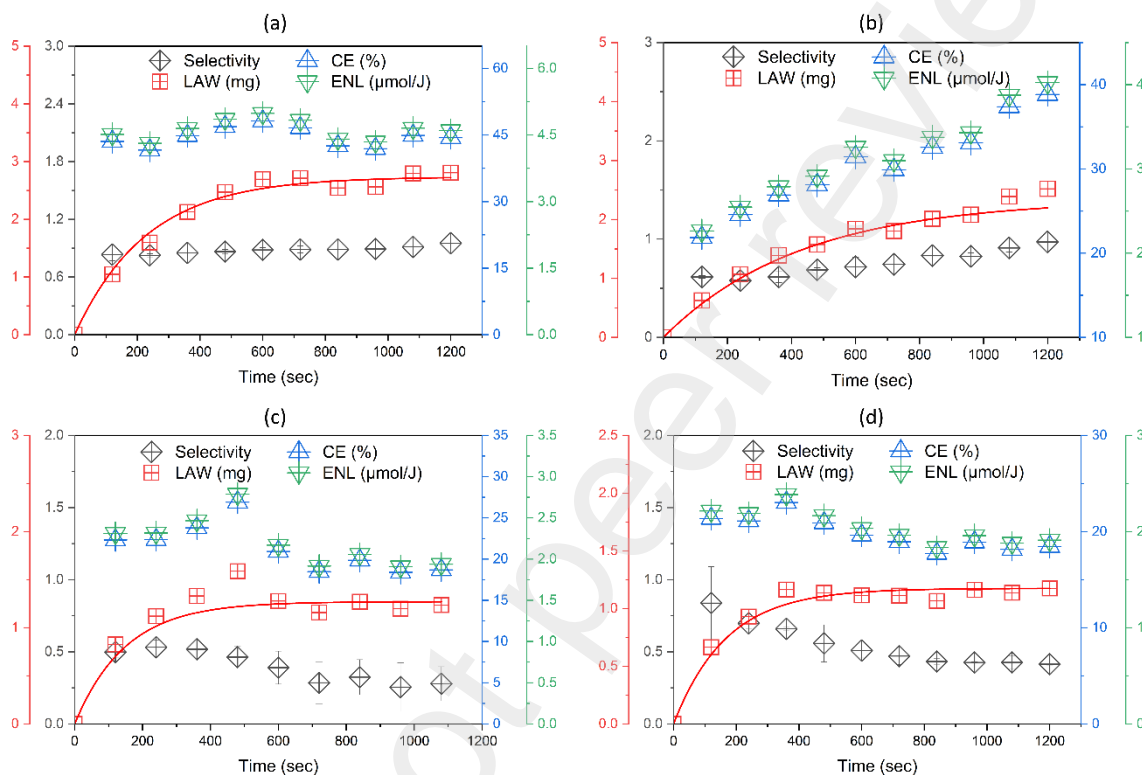
322 In our previous study on the CDI performance of bare AC electrodes, binary feed solutions and
 323 a CV of 1.0 V were applied in the CDI tests [50]. Similarly, the same feed solution components
 324 and charge potential conditions were employed to investigate the MCDI performance
 325 incorporating ZIF-8-PDA. The ion removal performance is illustrated in **Fig. S1**. The
 326 concentrations of all cations decreased, and the ion removal rates increased with the
 327 electrosorption duration, then both remained at a certain level, indicating the saturation of ion
 328 adsorption. Finally, the removal rates of all competing ions, i.e., Na, K, Mg, and Ca, were at a
 329 similar level, reaching 22.20%, 18.89%, 21.16%, and 20.27%, respectively. However, the Li

330 removal rate varied in monovalent and divalent cases. The η_{Li} reached 21.11% and 18.37% in
331 Na and K competing cases, respectively, yet were 6.08% and 8.39% when Mg and Ca coexisted.
332 **Fig. S2** presents the conductivity and pH of the solutions during the adsorption and desorption
333 processes. The conductivity in the solutions lowered gradually with the reduction of metal ions
334 and then kept steady, implying the completion of adsorption. Conversely, in the desorption
335 period, the conductivity rose rapidly in the beginning 5 mins with the release of ions and then
336 remained steady at 450-550 $\mu\text{S}/\text{cm}$. The pH raised and reduced slightly in the adsorption and
337 desorption stages, respectively, which could be explained by the electrosorption and release of
338 protons. The metrics of Li selectivity, CE, LAW, and ENL for the ZIF-8-PDA coated AC
339 electrodes are displayed in **Fig.8**. LAW rose till it reached a saturated level defined as LAC.
340 LAC was over double in monovalent cases than in divalent cases. Li selectivity (ρ_M^{Li}) can reflect
341 the ability to separate Li from binary solutions. Here, ρ_{Na}^{Li} , ρ_K^{Li} , ρ_{Mg}^{Li} , and ρ_{Ca}^{Li} were estimated to
342 be 0.95, 0.97, 0.28, and 0.41, respectively.

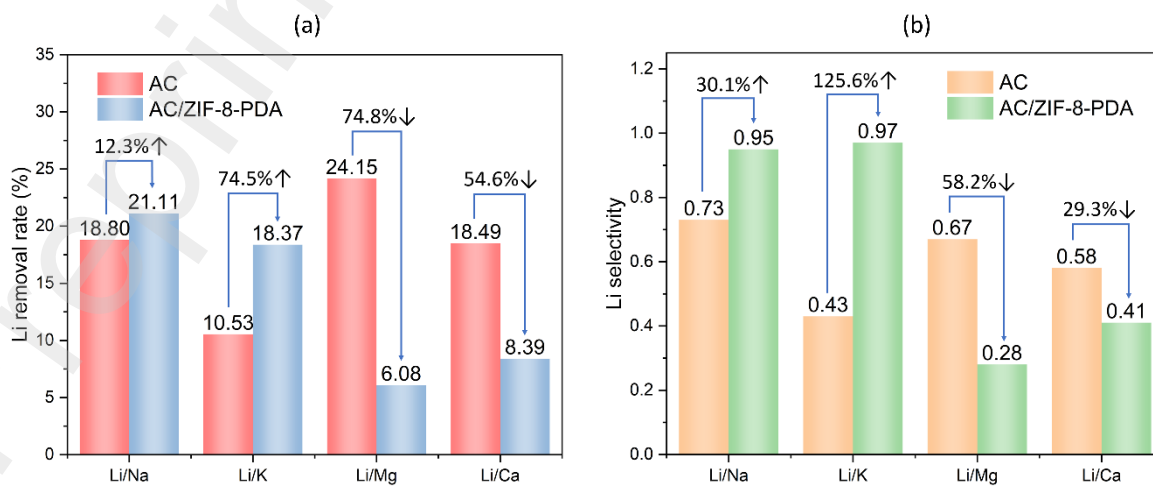
343 Compared to the bare AC electrodes [50], the Li removal rates augmented by 12.3% and 74.5%
344 in Na and K coexisting feeds and decreased by 74.8% and 54.6% in Mg and Ca coexisting
345 feeds, respectively; Li selectivity to Na and K improved by 30.1% and 125.6%, and those to
346 Mg and Ca declined by 58.2% and 29.3%, respectively (see **Fig. 9**). The presence of ZIF-8-
347 PDA built up the preference of electrodes to Li in monovalent cases. Hou and Huang reported
348 that monovalent cations with lower dehydration enthalpy were favorable to be electrosorbed in
349 an AC electrode-based CDI system [70]. However, the size-sieving role of the ZIF-8-PDA
350 layer can promote the monovalent cations with smaller dehydrated ion radius to pass through
351 the membrane. In monovalent and divalent cation mix situations, cations with higher valences
352 are more sensitive in an electric field due to stronger electrostatic attractions. The ZIF-8-PDA
353 membrane as a barrier layer magnified the influence of charge potentials on valences, further
354 facilitating divalent ions to permeate the membrane in priority. However, compared to AC/ZIF-
355 8 electrodes [50], although the water stability improved with the presence of PDA, Li
356 selectivity generally dropped, mainly caused by the increase in pore sizes. Thus, the trade-off
357 between Li selectivity and water stability should be noticed.

358 CE and ENL were calculated according to the measured current, power, resistance, and
359 electrical charge (shown in **Fig. S3**). These parameters give insight into charge and energy
360 consumption on Li adsorption from the mixed feed stream of the MCDI system. Charges used
361 for achieving Li extraction are considered effective usage, while those consumed by competing
362 ions and electrodes are regarded as charge loss. ENL reflects on the moles of captured Li per

363 joule energy input. The CE and ENL were computed to be 44.4% and 4.60 $\mu\text{mol}/\text{J}$ in Li/Na
 364 binary feed, 38.8% and 4.03 $\mu\text{mol}/\text{J}$ in Li/K binary feed, 18.7% and 1.94 $\mu\text{mol}/\text{J}$ in Li/Mg
 365 binary feed, and 18.4% and 1.91 $\mu\text{mol}/\text{J}$ in Li/Ca binary feed, respectively. Consistent with
 366 LAC and Li selectivity, CE and ENL were markedly higher in monovalent than divalent cases,
 367 implying that more Li were extracted per unit of energy input to the monovalent feed MCDI
 368 system.



369
 370 **Figure 8.** Temporal Li extraction performances of Li selectivity, LAW, CE, and ENL of ZIF-
 371 8-PDA coated CDI under 1.0V by using binary feed solution of (a) Li+Na, (b) Li+K, (c) Li+Mg,
 372 and (d) Li+Ca mixes.



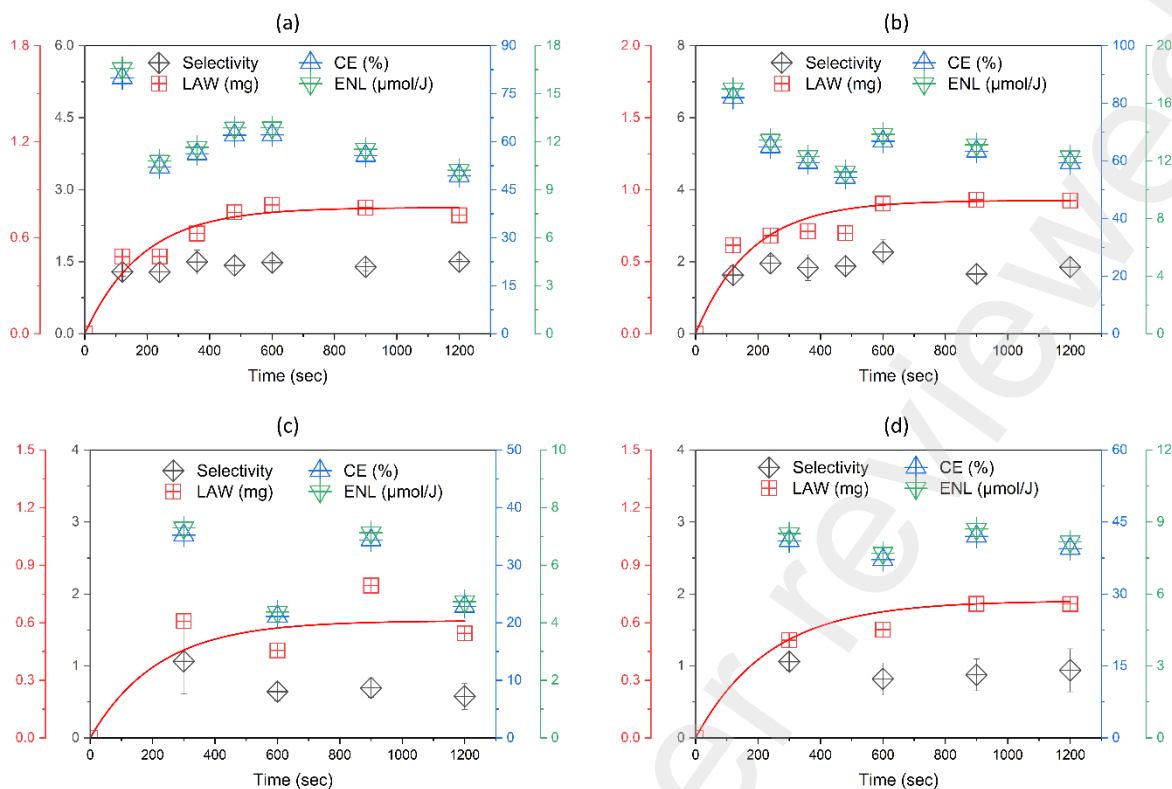
373

374 **Figure 9.** The changes of (a) Li removal rates and (b) Li selectivity after coating ZIF-8-PDA
375 on AC electrodes.

376 3.3.2 MCDI performance under 0.5 V

377 The value of applied charge potential could be one of the most critical parameters influencing
378 the MCDI performance. To investigate the Li extraction performance under different voltages,
379 0.5 V and 1.5 V of constant voltages were also applied for the AC/ZIF-8-PDA electrode-based
380 MCDI system. According to the results of 1.0 V tests, a higher potential was presented to
381 extract Li from the feed with monovalent-ion coexistence, and the electrode saturation
382 durations were within 10 mins for both monovalent and divalent cases. Therefore, in the tests
383 under 0.5 V and 1.5 V, samples were collected every 2 mins in the first 10 mins and every 5
384 mins in the last 10 mins for monovalent cases, and every 5 mins in the whole electrosorption
385 duration for divalent cases.

386 The results of ion removal rates and Li extraction performance under 0.5 V are presented in
387 **Fig. S4 and 10.** Qualitatively, Li extraction performance in monovalent cases was ascendant
388 than in divalent cases, consistent with the results under 1.0 V. For Li/Na and Li/K binary feed,
389 the corresponding Li removals were 13.7% and 20.5%, and Na and K removals were 9.1% and
390 11.0%, realizing Li selectivity of 1.50 and 1.85, respectively. For Li/Mg and Li/Ca binary feed,
391 Li removals were 7.0% and 14.5%, while Mg and Ca removals were 12.0% and 15.7%,
392 corresponding Li selectivity of 0.58 and 0.94, respectively. The reduced applied voltage
393 provided weaker external stimuli for cations to span the membrane, causing the values of LAC
394 to drop substantially. The conductivity and pH information in adsorption and desorption
395 processes are shown in **Fig. S5.** Since fewer amounts of metal ions were adsorbed when
396 applying the lower voltage, the final conductivity in desorption processes were also low, no
397 higher than 300 $\mu\text{S}/\text{cm}$. On the other hand, the pH of solutions under 0.5 V remained steady
398 since the electrodes adsorbed a small number of protons. According to the charge information
399 shown in **Fig. S6,** CE and ENL for Na, K, Mg, and Ca coexisting feeds were estimated to be
400 49.3% and 10.22 $\mu\text{mol}/\text{L}$, 59.3% and 12.30 $\mu\text{mol}/\text{L}$, 22.8% and 4.73 $\mu\text{mol}/\text{L}$, and 39.5% and
401 8.18 $\mu\text{mol}/\text{L}$, respectively. More analysis of the influence of applied voltages is discussed in
402 section 3.3.4.



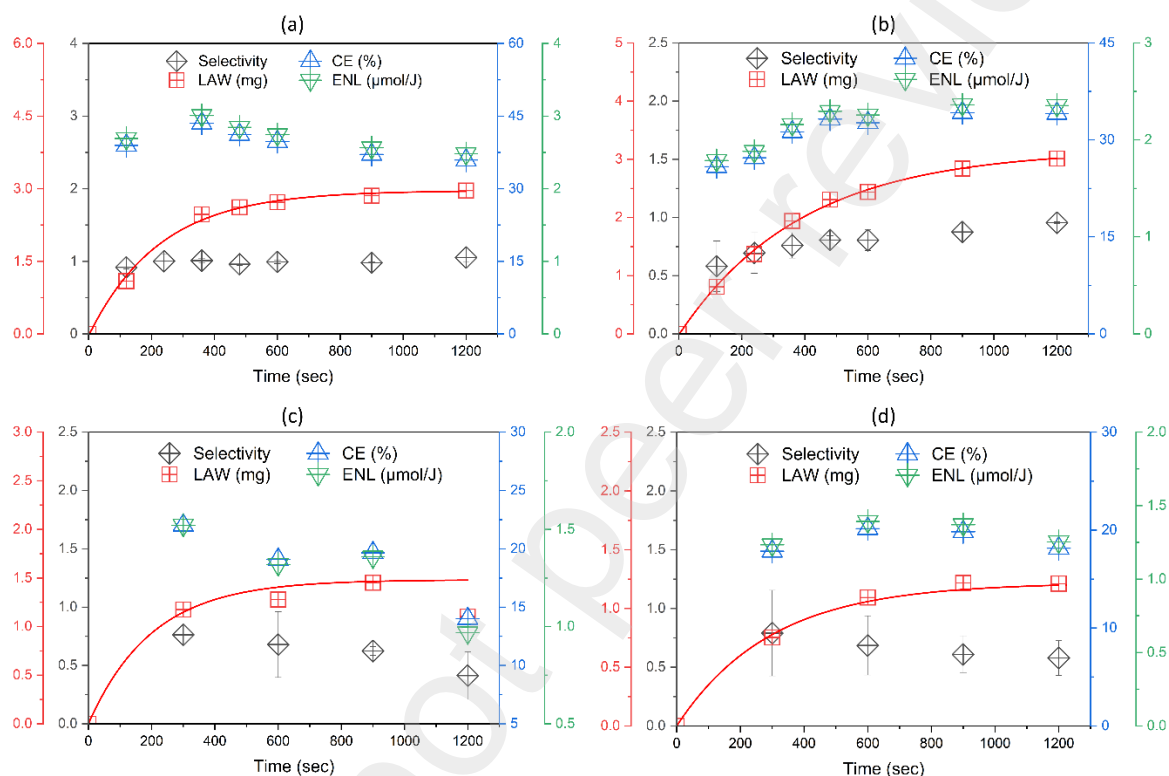
403

404 **Figure 10.** Temporal Li extraction performances of Li selectivity, LAW, CE, and ENL of ZIF-
 405 8-PDA coated CDI under 0.5V by using binary feed solution of (a) Li+Na, (b) Li+K, (c) Li+Mg,
 406 and (d) Li+Ca mixes.

407 3.3.3 MCDI performance under 1.5 V

408 The results of ion removal rates and Li extraction performance under 1.5 V are presented in
 409 **Fig. S7 and 11.** The removal rates of Li and the coexisting cation were approximative in
 410 monovalent cases, with 23.6% and 23.6% of Li and Na removal rates, respectively, and 24.1%
 411 and 24.1% of Li and K removal rates, respectively. Correspondingly, LAC and Li selectivity
 412 were estimated to be 2.98 mg and 1.05 in Li/Na feed and 3.01 mg and 0.95 in Li/K feed,
 413 respectively. In divalent cases, Li removal rates were distinctly lower than Mg and Ca removal
 414 rates. The ion removal rates of Li and Mg were 8.9% and 21.3%, respectively, and those of Li
 415 and Ca were 11.1% and 19.0%, respectively. Accordingly, LAC and Li selectivity in Li/Mg
 416 feed were calculated to be 1.10 mg and 0.41, slightly lower than in Li/Ca feed of 1.21 mg and
 417 0.58, respectively. The conductivity and pH values in the adsorption and desorption processes
 418 are demonstrated in **Fig. S8.** The reduction and increase of the conductivity in ad- and
 419 desorption processes under 1.5 V were close to those under 1.0 V. The pH values rose slightly
 420 during the electrosorption process. Notably, the increase was higher in monovalent cases than
 421 in divalent cases. During desorption processes, the pH values dropped marginally in

422 monovalent cases yet stayed steady in divalent cases. CE and ENL were computed according
 423 to the charge data in **Fig. S9**. 35.9% and 34.1% of consumed charge were applied for Li capture
 424 in Li/Na and Li/K feeds, respectively, which were nearly double than CE in Li/Mg (14.0%)
 425 and Li/Ca (18.1%) feeds. 2.48 μmol and 2.35 μmol of Li were uptaken with every joule energy
 426 input into Li/Na and Li/K feeds, respectively, yet only 0.97 μmol and 1.25 μmol of Li were
 427 gained with per joule energy input into Li/Mg and Li/Ca feeds, respectively. More discussion
 428 about the evaluation of Li extraction performance is elaborated in section 3.3.4.



429
 430 **Figure 11.** Temporal Li extraction performances of Li selectivity, LAW, CE, and ENL of ZIF-
 431 8-PDA coated CDI under 1.5V by using binary feed solution of (a) Li+Na, (b) Li+K, (c) Li+Mg,
 432 and (d) Li+Ca mixes.

433 3.3.4 Comparison of MCDI performance under different voltages

434 In sections 3.3.1 to 3.3.3, MCDI results under 0.5 V, 1.0 V, and 1.5 V are displayed and
 435 compared in terms of coexisting ions. In general, monovalent cases presented distinct
 436 advantages for Li capture over divalent cases under these three voltages. The Li selectivity,
 437 LAC, CE, and ENL in Li/Na feeds were over 2.5, 1.4, 2.2, and 2.2 times those in Li/Mg feeds,
 438 respectively; those in Li/K feeds were over 1.7, 1.3, 1.5, and 1.5 times those in Li/Ca feeds.
 439 Additionally, for the competing cations with the same valences, the competitiveness could
 440 depend on bare ion radius and dehydration enthalpy. The Li extraction performances in Li/K

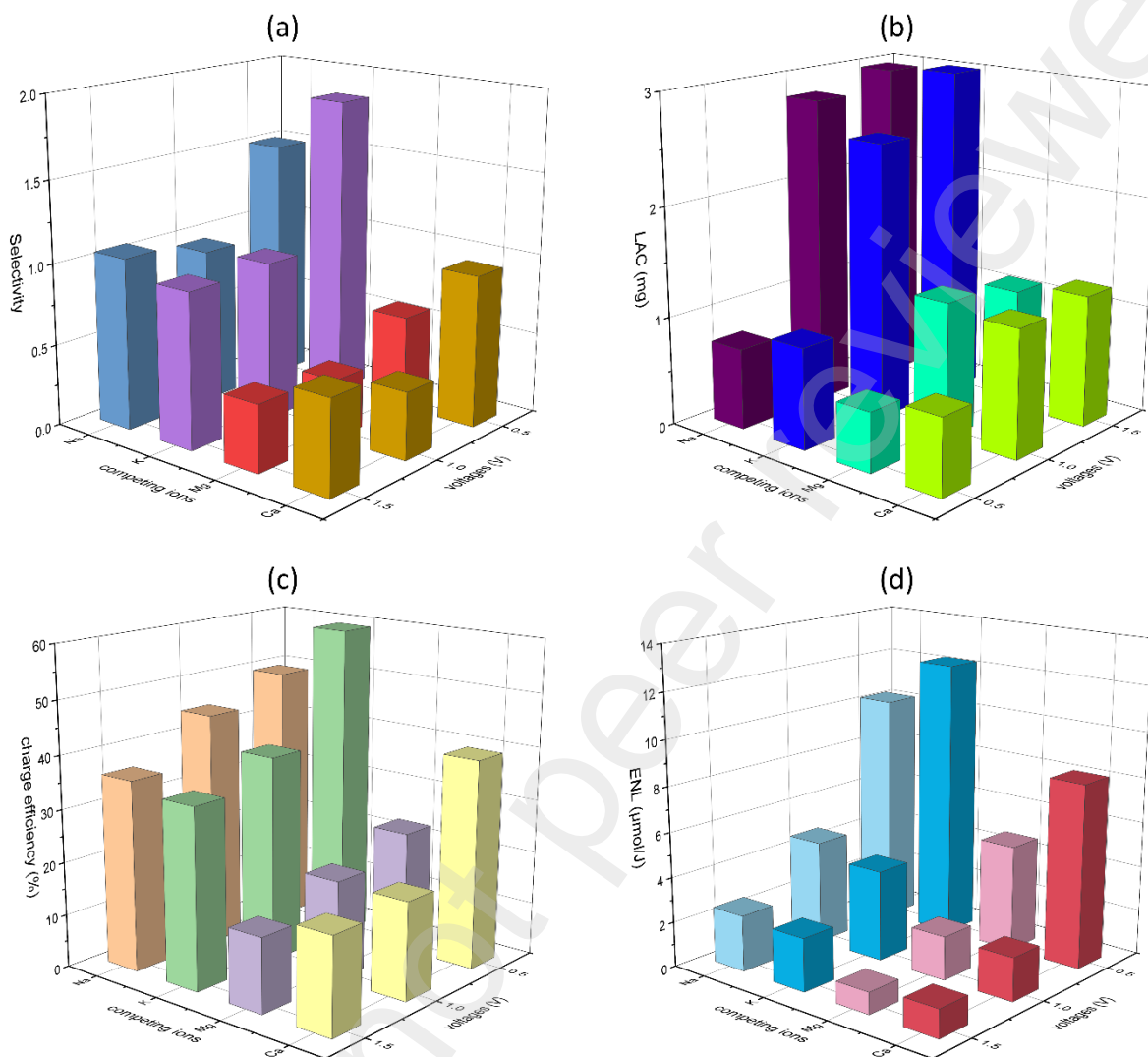
441 and Li/Ca cases could be marginally superior to Li/Na and Li/Mg, respectively. The
442 phenomena denoted that ion size, dehydration enthalpy, and valence could jointly determine
443 ion selectivity under an electric field. In particular, the valence exhibited a more substantial
444 influence than the ion size.

445 **Fig. 12** concludes and compares Li extraction performances of AC/ZIF-8-PDA electrode-based
446 MCDI under three different voltages. Overall, the metrics of Li selectivity, CE, and ENL
447 exhibited better behaviors under lower voltages, but conversely, LAC became higher with the
448 increase of voltages. **Fig. 12(a)** indicated a similarity of Li selectivity and a cation adsorption
449 order of $K \approx Na \approx Li < Ca < Mg$ under 1.0 V and 1.5 V. However, Li selectivity conspicuously
450 increased to 1.4-1.9 times when the voltage lowered to 0.5 V, and the cation adsorption order
451 switched to $K < Na < Li < Ca < Mg$. Notably, Li selectivity in monovalent cases exceeded 1.5
452 under 0.5 V, accomplishing 1.50 to Na and 1.85 to K. It might be because the cations with
453 larger sizes need stronger driven force to squeeze into the membrane pores, but a reduced
454 voltage could not provide enough stimuli. Under a lower voltage, fewer cations could be
455 pushed into the membrane pores, and smaller ones were preferred. In other words, the influence
456 of charge potentials was more significant to cations with larger sizes. The ion removal rates of
457 larger-size cations reduced more than Li when decreasing the voltages, resulting in improved
458 Li selectivity.

459 Similar to Li selectivity, as shown in **Fig. 12(b)**, the difference between LAC under 1.0 V and
460 1.5 V could also be neglectable. Contrary to Li selectivity, LAC under 1.0 V and 1.5 V was
461 significantly greater than that under 0.5 V. The charge potential was the external stimuli that
462 drove Li-ions passing through and through the membrane layer. Under low voltages, a small
463 number of ions could effortlessly enter the nanopores due to the limited driven force; however,
464 with the increase of voltages, a stronger driven force could push more Li-ions overcoming the
465 restriction from the membrane. Nevertheless, the upper limit of electrode capacity and the
466 decrease of the marginal effect would cause insufficient LAC growths with a further voltage
467 increase from 1.0 V to 1.5 V.

468 For CE and ENL illustrated in **Fig. 12(c)** and **(d)**, they grew gradually with the diminution of
469 voltages. CE and values of ENL under 0.5 V were 1.4-2.2 times and 4.1-6.5 times those under
470 1.5 V, respectively. It was partially because water hydrolysis occurred when the voltage was
471 over 1.23 V and consumed more energy. In summary, applying a low voltage could achieve

472 higher Li selectivity, CE, and ENL, demonstrating a potential for Li extraction with low energy
473 inputs.



474
475 **Figure 12.** The comparison of Li extraction performance in binary solutions for (a) Li
476 selectivity, (b) LAC, (c) CE, and (d) ENL of ZIF-8-PDA coated MCDI by charge potentials
477 and competing cations.

478 4. Conclusions and perspectives

479 The rapid increase in Li demand requires effective and energy-saving techniques to extract Li
480 from aqueous resources. In this study, AC electrodes were coated by ZIF-8-PDA membrane
481 via the deposition coating method. ZIF-8 particles displayed great water stability with the
482 protection of PDA. The modified electrodes were assembled in the MCDI system for Li
483 extraction from diluted binary solutions containing Li and Na/K/Mg/Ca. The performance of
484 Li extraction was evaluated regarding Li selectivity, LAC, CE, and ENL. The constant voltages

485 of 0.5 V, 1.0 V, and 1.5 V were applied to investigate the influence of charge potentials on Li
486 extraction performances. The main findings of the electrosorption experiments are summarized
487 as follows:

- 488 1) The presence of ZIF-8-PDA on AC electrodes enhanced Li removal rates and Li selectivity
489 in Li/Na and Li/K binary solutions substantially but declined those in Li/Mg and Li/Ca
490 binary solutions.
- 491 2) The performance of Li extraction in monovalent cases presented superior results than in
492 divalent cases, which could be triggered by the sensitivity of valences to the electric field.
493 The ion size and dehydration enthalpy could also influence Li selectivity. The MCDI
494 system showed a slight preference for cations with smaller bare radii compared to larger
495 ones with the same valence.
- 496 3) The applied voltages demonstrated negative relationships with Li selectivity, CE, and ENL.
497 Li selectivity, CE, and ENL under 0.5 V were approximately 1.4-1.9, 1.4-2.1, and 4.1-6.5
498 times those under 1.5 V, respectively. Li selectivity in Li/Na and Li/K feeds accomplished
499 1.50 and 1.85 under 0.5 V, confirming the potential to selectively extract Li from SWRO
500 brine with low energy input.
- 501 4) LAC increased greatly when the voltage raised from 0.5 V to 1.0 V, yet a higher voltage
502 could not instigate further growth of LAC.

503 For clear pair comparisons of Li and its competing ions, equimolar binary solutions were used
504 as feeds for MCDI tests in this study. However, the compositions and concentrations of cations
505 in real-world brine are more complicated and diverse. In future work, it is necessary to
506 investigate the performances of Li extraction using multi-component model solutions and
507 simulated brine as feeds.

508

509 **Declaration of competing interest**

510 The authors declare that they have no known competing financial interests or personal
511 relationships that could have appeared to influence the work reported in this paper.

512 Acknowledgments

513 This research was supported by grants from the Australian Research Council (ARC) Discovery
514 Projects (DP230100238) and the Qatar National Research Fund under its National Priorities
515 Research Program (NPRP 12S-0227-190166).

516

517 References

- 518 1. Yang, S., et al., *Lithium Metal Extraction from Seawater*. Joule, 2018. **2**(9): p. 1648-
519 1651.
- 520 2. Grosjean, C., et al., *Assessment of world lithium resources and consequences of their*
521 *geographic distribution on the expected development of the electric vehicle industry*.
522 *Renewable and Sustainable Energy Reviews*, 2012. **16**(3): p. 1735-1744.
- 523 3. USGS, *Mineral Commodity Summaries 2022*, in *Mineral Commodity Summaries*. 2022,
524 U.S. Geological Survey.
- 525 4. Yu, H., et al., *Metal-based adsorbents for lithium recovery from aqueous resources*.
526 *Desalination*, 2022. **539**(115951).
- 527 5. Li, X., et al., *Membrane-based technologies for lithium recovery from water lithium*
528 *resources: A review*. *Journal of Membrane Science*, 2019. **591**(117317).
- 529 6. Coterillo, R., et al., *Selective extraction of lithium from seawater desalination*
530 *concentrates: Study of thermodynamic and equilibrium properties using Density*
531 *Functional Theory (DFT)*. *Desalination*, 2022. **532**(115704).
- 532 7. Orooji, Y., et al., *Recent advances in nanomaterial development for lithium ion-sieving*
533 *technologies*. *Desalination*, 2022. **529**(115624).
- 534 8. Battistel, A., et al., *Electrochemical Methods for Lithium Recovery: A Comprehensive*
535 *and Critical Review*. *Adv Mater*, 2020. **32**(1905440).
- 536 9. Liu, D., et al., *A closed-loop process for selective lithium recovery from brines via*
537 *electrochemical and precipitation*. *Desalination*, 2021. **519**(115302).
- 538 10. Perez-Antolin, D., et al., *Regenerative electrochemical ion pumping cell based on semi-*
539 *solid electrodes for sustainable Li recovery*. *Desalination*, 2022. **533**(115764).
- 540 11. Zavahir, S., et al., *A review on lithium recovery using electrochemical capturing*
541 *systems*. *Desalination*, 2021. **500**(114883).
- 542 12. Xu, Y., et al., *High performance Mg²⁺/Li⁺ separation membranes modified by a bis-*
543 *quaternary ammonium salt*. *Desalination*, 2022. **526**(115519).

- 544 13. He, R., et al., *Unprecedented Mg²⁺/Li⁺ separation using layer-by-layer based*
545 *nanofiltration hollow fiber membranes*. Desalination, 2022. **525**(115492).
- 546 14. Gong, L., et al., *Direct numerical simulation of continuous lithium extraction from high*
547 *Mg²⁺/Li⁺ ratio brines using microfluidic channels with ion concentration polarization*.
548 *J Memb Sci*, 2018. **556**: p. 34-41.
- 549 15. Bazrgar Bajestani, M., A. Moheb, and M. Dinari, *Preparation of lithium ion-selective*
550 *cation exchange membrane for lithium recovery from sodium contaminated lithium*
551 *bromide solution by electrodialysis process*. Desalination, 2020. **486**(114476).
- 552 16. Sharma, P.P., et al., *Sulfonated poly (ether ether ketone) composite cation exchange*
553 *membrane for selective recovery of lithium by electrodialysis*. Desalination, 2020.
554 **496**(114755).
- 555 17. M. Bryjak, A.S., J. Kujawski, K. Smolinska-Kempisty, W. Kujawski, *Capacitive*
556 *deionization for selective extraction of lithium from aqueous solutions*. *Journal of*
557 *Membrane and Separation Technology*, 2015. **4**: p. 110-115.
- 558 18. Sahin, S., et al., *Enhanced monovalent over divalent cation selectivity with*
559 *polyelectrolyte multilayers in membrane capacitive deionization via optimization of*
560 *operational conditions*. Desalination, 2022. **522**(115391).
- 561 19. Chen, Z., et al., *Ultra-durable and highly-efficient hybrid capacitive deionization by*
562 *MXene confined MoS₂ heterostructure*. Desalination, 2022. **528**(115616).
- 563 20. Xing, W., et al., *Versatile applications of capacitive deionization (CDI)-based*
564 *technologies*. Desalination, 2020. **482**(114390).
- 565 21. Liu, X., et al., *Cost Comparison of Capacitive Deionization and Reverse Osmosis for*
566 *Brackish Water Desalination*. *ACS ES&T Engineering*, 2020. **1**(2): p. 261-273.
- 567 22. Choi, J., et al., *Applications of capacitive deionization: Desalination, softening,*
568 *selective removal, and energy efficiency*. Desalination, 2019. **449**: p. 118-130.
- 569 23. Gamaethiralalage, J.G., et al., *Recent advances in ion selectivity with capacitive*
570 *deionization*. *Energy & Environmental Science*, 2021. **14**(3): p. 1095-1120.
- 571 24. Chen, T.H., et al., *Cation selectivity of activated carbon and nickel hexacyanoferrate*
572 *electrode materials in capacitive deionization: A comparison study*. *Chemosphere*,
573 2022. **307**(135613).
- 574 25. Suss, M.E., et al., *Water desalination via capacitive deionization: what is it and what*
575 *can we expect from it?* *Energy & Environmental Science*, 2015. **8**(8): p. 2296-2319.
- 576 26. Porada, S., et al., *Direct prediction of the desalination performance of porous carbon*
577 *electrodes for capacitive deionization*. *Energy & Environmental Science*, 2013. **6**(12).

- 578 27. Hu, B., et al., *Lithium ion sieve modified three-dimensional graphene electrode for*
579 *selective extraction of lithium by capacitive deionization*. J Colloid Interface Sci, 2022.
580 **612**: p. 392-400.
- 581 28. Oyarzun, D.I., et al., *Ion selectivity in capacitive deionization with functionalized*
582 *electrode: Theory and experimental validation*. Water Res X, 2018. **1**(100008).
- 583 29. Shang, X., et al., *LiNi_{0.5}Mn_{1.5}O₄-based hybrid capacitive deionization for highly*
584 *selective adsorption of lithium from brine*. Separation and Purification Technology,
585 2021. **258**(118009).
- 586 30. Kim, B., J.Y. Seo, and C.-H. Chung, *Electrochemical Desalination and Recovery of*
587 *Lithium from Saline Water upon Operation of a Capacitive Deionization Cell*
588 *Combined with a Redox Flow Battery*. ACS ES&T Water, 2021. **1**(4): p. 1047-1054.
- 589 31. Shang, X., et al., *Synthesis of lithium vanadate/reduced graphene oxide with strong*
590 *coupling for enhanced capacitive extraction of lithium ions*. Separation and Purification
591 Technology, 2021. **262**(118294).
- 592 32. Jin, W., et al., *Simultaneous and precise recovery of lithium and boron from salt lake*
593 *brine by capacitive deionization with oxygen vacancy-rich CoP/Co₃O₄-graphene*
594 *aerogel*. Chemical Engineering Journal, 2021. **420**(127661).
- 595 33. Siekierka, A., *Lithium iron manganese oxide as an adsorbent for capturing lithium ions*
596 *in hybrid capacitive deionization with different electrical modes*. Separation and
597 Purification Technology, 2020. **236**(116234).
- 598 34. Ha, Y., et al., *Continuous Lithium Extraction from Aqueous Solution Using Flow-*
599 *Electrode Capacitive Deionization*. Energies, 2019. **12**(15).
- 600 35. Siekierka, A., *Lithium and magnesium separation from brines by hybrid capacitive*
601 *deionization*. Desalination, 2022. **527**(115569).
- 602 36. Siekierka, A. and M. Bryjak, *Selective sorbents for recovery of lithium ions by hybrid*
603 *capacitive deionization*. Desalination, 2021. **520**(115324).
- 604 37. Siekierka, A., B. Tomaszewska, and M. Bryjak, *Lithium capturing from geothermal*
605 *water by hybrid capacitive deionization*. Desalination, 2018. **436**: p. 8-14.
- 606 38. Xie, N., et al., *Fabricating a Flow-Through Hybrid Capacitive Deionization Cell for*
607 *Selective Recovery of Lithium Ions*. ACS Applied Energy Materials, 2021. **4**(11): p.
608 13036-13043.
- 609 39. Choi, J., H. Lee, and S. Hong, *Capacitive deionization (CDI) integrated with*
610 *monovalent cation selective membrane for producing divalent cation-rich solution*.
611 Desalination, 2016. **400**: p. 38-46.

- 612 40. Shi, W., et al., *Efficient lithium extraction by membrane capacitive deionization*
613 *incorporated with monovalent selective cation exchange membrane*. Separation and
614 Purification Technology, 2019. **210**: p. 885-890.
- 615 41. Wang, S., et al., *Metal-Organic Framework Nanoparticles*. Adv Mater, 2018. **30**(37):
616 p. e1800202.
- 617 42. O. M. Yaghi, G.L., Hailian Li, *Selective binding and removal of guests in a microporous*
618 *metal–organic framework*. Nature, 1995. **378**(6558): p. 703–706.
- 619 43. Liu, Y., et al., *Zeolitic imidazolate framework-based nanomaterials for the capture of*
620 *heavy metal ions and radionuclides: A review*. Chemical Engineering Journal, 2021.
621 **406**(127139).
- 622 44. Kukkar, P., et al., *Recent advances in the synthesis techniques for zeolitic imidazolate*
623 *frameworks and their sensing applications*. Coordination Chemistry Reviews, 2021.
624 **446**(214109).
- 625 45. Arafat, Y., et al., *Advances in Zeolite Imidazolate Frameworks (ZIFs) Derived*
626 *Bifunctional Oxygen Electrocatalysts and Their Application in Zinc–Air Batteries*.
627 Advanced Energy Materials, 2021. **11**(26).
- 628 46. Liu, Y., et al., *The application of Zeolitic imidazolate frameworks (ZIFs) and their*
629 *derivatives based materials for photocatalytic hydrogen evolution and pollutants*
630 *treatment*. Chemical Engineering Journal, 2021. **417**(127914).
- 631 47. Chin, M., et al., *Rhodamine B degradation by nanosized zeolitic imidazolate*
632 *framework-8 (ZIF-8)*. RSC Adv, 2018. **8**(47): p. 26987-26997.
- 633 48. Zhang, H., et al., *Ultrafast selective transport of alkali metal ions in metal organic*
634 *frameworks with subnanometer pores*. Sci. Adv. , 2018. **4**(eaaq0066).
- 635 49. Mohammad, M., et al., *Metal-Phenolic network and metal-organic framework*
636 *composite membrane for lithium ion extraction*. Applied Materials Today, 2020.
637 **21**(100884).
- 638 50. Hossain, S.M., et al., *ZiF-8 induced carbon electrodes for selective lithium recovery*
639 *from aqueous feed water by employing capacitive deionization system*. Desalination,
640 2023. **546**(116201).
- 641 51. Zheng, W. and L.Y.S. Lee, *Metal–Organic Frameworks for Electrocatalysis: Catalyst*
642 *or Precatalyst?* ACS Energy Letters, 2021. **6**(8): p. 2838-2843.
- 643 52. Liu, X., et al., *Improvement of hydrothermal stability of zeolitic imidazolate*
644 *frameworks*. Chem Commun (Camb), 2013. **49**(80): p. 9140-9142.

- 645 53. Zhang, H., et al., *Improving hydrostability of ZIF-8 membranes via surface ligand*
646 *exchange*. Journal of Membrane Science, 2017. **532**: p. 1-8.
- 647 54. Zhang, M.-y., et al., *Improving the hydrostability of ZIF-8 membrane by biomolecule*
648 *towards enhanced nanofiltration performance for dye removal*. Journal of Membrane
649 Science, 2021. **618**(118630).
- 650 55. You, H., et al., *Advantages of polydopamine coating in the design of ZIF-8-filled thin-*
651 *film nanocomposite (TFN) membranes for desalination*. Colloids and Surfaces A:
652 Physicochemical and Engineering Aspects, 2021. **629**(127492).
- 653 56. H. Lee, S.M.D., W.M. Miller, P.B. Messersmith, *Mussel-Inspired Surface Chemistry*
654 *for Multifunctional Coatings*. Science, 2007. **318**: p. 426-430.
- 655 57. Wu, X., et al., *Polydopamine tethered enzyme/metal-organic framework composites*
656 *with high stability and reusability*. Nanoscale, 2015. **7**(45): p. 18883-18886.
- 657 58. Tian, Q., et al., *Polydopamine-stabilized ZIF-8: Improved water stability and*
658 *lubrication performance*. Applied Surface Science, 2022. **578**(152120).
- 659 59. Sánchez-Láinez, J., et al., *Influence of ZIF-8 particle size in the performance of*
660 *polybenzimidazole mixed matrix membranes for pre-combustion CO₂ capture and its*
661 *validation through interlaboratory test*. Journal of Membrane Science, 2016. **515**: p.
662 45-53.
- 663 60. Mei, X., et al., *Improving the Selectivity of ZIF-8/Polysulfone-Mixed Matrix*
664 *Membranes by Polydopamine Modification for H₂/CO₂ Separation*. Front Chem, 2020.
665 **8**: p. 528.
- 666 61. Zhang, H., et al., *Stability of ZIF-8 membranes and crystalline powders in water at*
667 *room temperature*. Journal of Membrane Science, 2015. **485**: p. 103-111.
- 668 62. Zhang, H., M. Zhao, and Y.S. Lin, *Stability of ZIF-8 in water under ambient conditions*.
669 Microporous and Mesoporous Materials, 2019. **279**: p. 201-210.
- 670 63. Zhang, H., et al., *Hydrolysis and condensation of ZIF-8 in water*. Microporous and
671 Mesoporous Materials, 2019. **288**.
- 672 64. Jr., E.R.N., *Phenomenological theory of ion solvation. Effective radii of hydrated ions*.
673 J. Phys. Chem., 1959. **63**(9): p. 1381-1387.
- 674 65. Smith, D.W., *Ionic Hydration Enthalpies*. Journal of Chemical Education, 1977. **54**(9):
675 p. 540.
- 676 66. Seo, S.J., et al., *Investigation on removal of hardness ions by capacitive deionization*
677 *(CDI) for water softening applications*. Water Res, 2010. **44**(7): p. 2267-2275.

- 678 67. Huang, D., et al., *Synergistic effects of zeolite imidazole framework@graphene oxide*
679 *composites in humidified mixed matrix membranes on CO₂ separation*. RSC Adv, 2018.
680 **8**(11): p. 6099-6109.
- 681 68. Dong, L., et al., *Metal-organic framework-graphene oxide composites: A facile method*
682 *to highly improve the CO₂ separation performance of mixed matrix membranes*.
683 *Journal of Membrane Science*, 2016. **520**: p. 801-811.
- 684 69. Yang, L., B. Tang, and P. Wu, *Metal-organic framework-graphene oxide composites:*
685 *a facile method to highly improve the proton conductivity of PEMs operated under low*
686 *humidity*. *Journal of Materials Chemistry A*, 2015. **3**(31): p. 15838-15842.
- 687 70. Hou, C.-H. and C.-Y. Huang, *A comparative study of electrosorption selectivity of ions*
688 *by activated carbon electrodes in capacitive deionization*. *Desalination*, 2013. **314**: p.
689 124-129.

690